ACS OMEGA

http://pubs.acs.org/journal/acsodf

Article

Crystallographic and Theoretical Exploration of Weak Hydrogen Bonds in Arylmethyl *N*′-(adamantan-1-yl)piperidine-1-carbothioimidates and Molecular Docking Analysis

Aamal A. Al-Mutairi, Kowsalya Alagappan, Olivier Blacque, Monirah A. Al-Alshaikh, Ali A. El-Emam, M. Judith Percino, and Subbiah Thamotharan*

Cite This: *ACS Omega* 2021, 6, 27026−27037

Read Online

ACCESS | Metrics & More | Article Recommendations | Supporting Information

ABSTRACT: Crystal structures of two potential chemotherapeutic agents, namely 4-nitrobenzyl *N*′-(adamantan-1-yl)piperidine-1-carbothioimidate **1** and 4-bromobenzyl *N*′-(adamantan-1-yl)piperidine-1-carbothioimidate **2**, have been analyzed in detail. X-ray analysis reveals that the molecular conformations of these compounds are strikingly different. These two structures are compared with two of their closely related structures. In the related structures, morpholine replaces piperidine. Based on the Hirshfeld surface analysis and two-dimensional (2D) fingerprint plots, we describe the effects of piperidine/morpholine and Br/NO_2 groups on the intermolecular interactions. An analysis of the CLP-PIXEL energy provides insight into the energetics of the dimers observed in the title compounds and their related structures. Compound **1** stabilizes with bifurcated C−H···S, C−H···O, and O(lp)···C(π) interactions, whereas compound **2** stabilizes with C−H···N, C−H···Br, and C−H···C interactions. The energy frameworks for the crystal structures of the title compounds reveal differences. The atoms-in-molecules (AIM) analysis was performed to confirm the intermolecular interactions found in the crystal structures of **1** and **2**. Additionally, docking analysis suggests that the title compounds bind at the active site of human sphingosine kinase 1, a well-known cancer target.

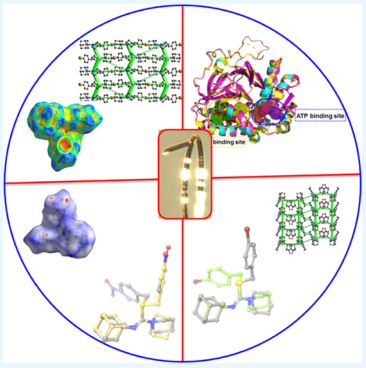

1. INTRODUCTION

The adamantane cage constitutes the essential building motif in several drugs.[1−4] The chemotherapeutic potency of adamantane-based derivatives was initially discovered after discovery of amantadine[5,6] and rimantadine[7] as effective therapies against Influenza A viral infections. Tromantadine was further developed as a potent antiviral drug to treat skin infections caused by the herpes simplex virus.[8] Adamantane-based derivatives are currently utilized as efficient therapies for the treatment of various cancers. Adaphostin is a tyrosine kinase inhibitor displaying antiproliferative activity in leukemia, non-small-cell lung cancer, and prostate cancer.[9] CD437, an adamantane-based synthetic retinoid, was discovered as a promising anticancer drug that acts by inhibiting the DNA polymerase.[10] Adarotene (ST1926) was also developed as a potent anticancer drug that acts by inhibition of IκB kinase-β for the treatment of leukemia, lymphoma, and prostate cancer.[11] Opaganib (ABC294640) is a recently approved adamantane-based anticancer drug to treat patients suffering from advanced solid tumors.[12] Opaganib induces its anticancer activity via selective inhibition of sphingosine kinase-2 (SK2). Interestingly, opaganib recently proved as a promising candidate for the treatment of severe COVID-19 pneumonia.[13] Numerous adamantane-based compounds were proved to possess potent activity against pathogenic bacteria, mycobacteria, and fungi. The adamantyl diamine derivative SQ109 was developed as a new drug for the treatment of drug-resistant tuberculosis.[14] The related adamantane-linked dipiperidine derivative SQ609 was further discovered as a lead compound with potent action against *Mycobacterium tuberculosis*.[15]

On the other hand, thiourea and isothiourea derivatives were proved to possess diverse chemotherapeutic activities, including anticancer,[16,17] antiviral,[18,19] antituberculosis,[20] and antimalarial[21] activities. Following an interest in the chemotherapeutic,[22−26] structural, and energetic properties of the weak noncovalent interactions[27−31] of adamantane-based derivatives, the title adamantane-isothiourea hybrid derivatives **1** and **2** were synthesized and proved to possess potent broad-spectrum antibacterial and antiproliferative activities.[26]

Saeed et al. described the vibrational and structural properties of 1-(adamantane-1-carbonyl)-3-halophenyl thioureas, and the molecular conformation of these compounds was found to stabilize via an intramolecular N−H···O=C hydrogen bond.[32] The crystal structures of these compounds

Received: July 6, 2021
Accepted: September 24, 2021
Published: October 7, 2021

are stabilized by the intermolecular N−H···S and bifurcated N−H···O=C hydrogen bonds. Recently, the crystal structure of an adamantane−naphthyl thiourea conjugate has been elucidated.[33] The molecular conformation of this compound was locked by an intramolecular N−H···O=C hydrogen bond forming an S(6) motif. Further, a weak intermolecular C−H···S interaction generates a centrosymmetric dimer with the $R_2^2(14)$ ring. The structure and energetics of (*Z*)-3-(adamantan-1-yl)-1-(phenyl or 3-chlorophenyl)-*S*-(4-bromobenzyl)isothioureas have recently been described.[30] Further, an intramolecular C−H···N interaction stabilizes the molecular conformation of these compounds. Different kinds of weak noncovalent interactions, such as C−H···O,[34] C−H···S,[35] C−H···N,[36] C−H···C(π),[37,38] C−H···Br,[39] and lp···π[40,41] interactions, play essential roles in the self-assembly of molecules in the solid state. These weak interactions were observed in the title compounds, and their roles are described in the present study.

In the present study, we examine the molecular conformation and role of noncovalent interactions in the crystal packing of two adamantane-isothiourea derivatives, namely 4-nitrobenzyl *N*′-(adamantan-1-yl)piperidine-1-carbothioimidate (**1**), $C_{23}H_{31}N_3O_2S$, and 4-bromobenzyl *N*′-(adamantan-1-yl)piperidine-1-carbothioimidate (**2**), $C_{23}H_{31}BrN_2S$. These two structures are compared with those of two closely related structures, namely 4-nitrobenzyl (Z)-*N*′-(adamantan-1-yl)-morpholine-4-carbothioimidate (CSD refcode: REMHID)[24] and 4-bromobenzyl (Z)-*N*′-(adamantan-1-yl)morpholine-4-carbothioimidate (CSD refcode: KUBDET),[42] reported in the literature (Figure 1). In the reported structures, the

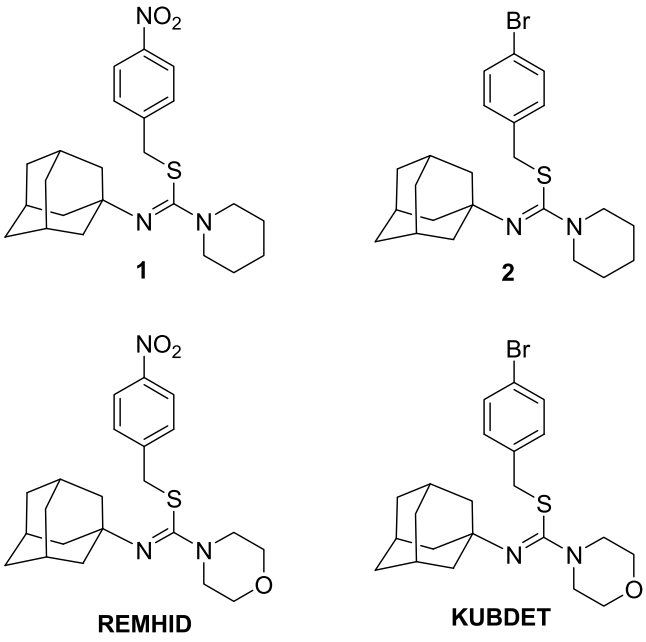

Figure 1. Structures of the investigated compounds **1** and **2**, and their morpholine analogues REMHID and KUBDET.

morpholine ring occupies the place of the piperidine ring moiety in **1** and **2**. The intermolecular interactions found in these crystal structures are characterized by Hirshfeld surfaces[43] and their decomposed 2D-fingerprint plots.[44] Additionally, different kinds of intermolecular interactions responsible for the formation of dimeric species are identified through the CLP-PIXEL energy analysis.[45,46] Further, dimers of structures **1** and **2** were subjected to the quantum theory of atoms in molecules (QTAIM)[47] topological analysis to study the nature and strength of weak intermolecular interactions. In addition, we describe a molecular docking analysis to show the potential of the title compounds against human sphigosine kinase 1 (SPHK1), a well-known target for cancer and inflammatory diseases.[48]

2. RESULTS AND DISCUSSION

2.1. Chemical Synthesis. The title compounds **1** and **2** were synthesized via condensation of adamantan-1-yl isothiocyanate **A** with piperidine **B** in ethanol to yield the corresponding *N*-(adamantan-1-yl)piperidine-1-carbothioamide **C**.[49] The carbothioamide **C** was then reacted with 4-nitrobenzyl bromide or 4-bromobenzyl bromide in *N*,*N*-dimethylformamide (DMF) in the presence of anhydrous potassium carbonate at room temperature, which yielded compounds **1** and **2**, respectively, in good yields (Scheme 1).[26] The ^{1}H and ^{13}C nuclear magnetic resonance (NMR) spectra of compounds **1** and **2** and the 2D, DEPT spectra of compound **1** are given in the Supporting Information (Figures S1−S8).

2.2. Crystal Structures. The crystal structures of compounds **1** and **2** were analyzed at 160 K to gain insights into their impact on molecular conformation, crystal packing, and intermolecular interactions. For comparison, two closely related structures, REMHID and KUBDET, were also used.

The X-ray diffraction studies of single crystals revealed that compound **1** crystallizes in the orthorhombic system with the space group $Pca2_1$, while compound **2** crystallizes in the monoclinic system with the space group $P2_1/c$. In both of these crystals, the asymmetric unit contains a single molecule (Z' = 1). Crystal data and refinement parameters for compounds **1** and **2** are summarized in Table 1. The thermal ellipsoid representation of compounds **1** and 2 is illustrated in Figure 2a and Figure 2b, respectively.

The X-ray analysis shows that the molecular conformation of compound **1** is somewhat bent, as evidenced by the torsion angle C8−S1−C7−C4. This torsion angle is 74.28° and is designated as a *syn*-clinal conformation in compound **1**. Two closely related structures, KUBDET (61.56°) and REMHID (73.09°), also exhibit folded conformation as observed in compound **1**. The structural superimposition diagram reveals that compound **2** adopts a different conformation than the other three structures (Figure 2c). The C8−S1−C7−C4 torsion angle is −175.14°, and this conformation is designated as *anti*-periplanar in compound **2**. The adamantyl moiety in all four compounds shows a chair conformation. The piperidine ring in compounds **1** and **2** and the morpholine ring in REMHID and KUBDET also adopt a chair conformation. Table S1 shows that bonds connecting adamantane, piperidine, and phenyl moieties are similar in length in **1** and **2** compared to their closely related structures. In **1** and **2**, the bridging S1−C7 bond has a slightly shorter length than it does in their closely related structures. However, another bridging C7−C4 bond in **2** is slightly longer compared to the other three structures. There may be a correlation between this lengthening and a different conformation exhibited by compound **2**. In addition, we noticed that the angle of S1−C7−C4 (108.25°) was shortened in **2** (108.25°) compared to the other three structures (112.42−113.12°).

To understand the conformational flexibility of compounds **1**, **2** and their closely related structures (REMHID and KUBDET), we performed single-point energy calculations and

https://doi.org/10.1021/acsomega.1c03559
ACS Omega 2021, 6, 27026−27037

Scheme 1. Synthetic Pathway for the Title Compounds 1 and 2

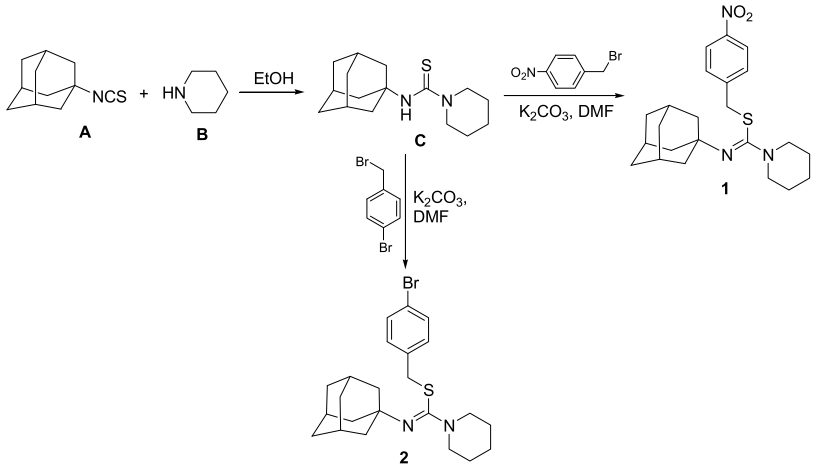

Table 1. Crystal Data and Structure Refinement Parameters for Compounds 1 and 2

	compound 1	compound 2
empirical formula	$C_{23}H_{31}N_3O_2S$	$C_{23}H_{31}BrN_2S$
formula weight	413.57	447.47
crystal system	orthorhombic	monoclinic
space group	$Pca2_1$	$P2_1/c$
temperature (K)	160 (1)	160 (1)
a (Å)	30.7924 (6)	9.55530 (10)
b (Å)	6.79420 (10)	9.32040 (10)
c (Å)	10.3886 (2)	24.2671 (3)
α (deg)	90	90
β (deg)	90	98.6060 (10)
γ (deg)	90	90
volume (Å^3)	2173.40 (7)	2136.88 (4)
Z	4	4
ρ_{calc} (g cm^{-3})	1.264	1.391
μ (mm^{-1})	1.506	3.595
$F(000)$	888.0	936.0
crystal size (mm^3)	0.24 × 0.07 × 0.02	0.4 × 0.17 × 0.03
radiation	Cu Kα, λ = 1.54184 Å	Cu Kα, λ = 1.54184 Å
2Θ range for data collection (deg)	5.74−148.996	7.368−148.98
index ranges	$-38 \le h \le 36$, $-8 \le k \le 8$, $-12 \le l \le 12$	$-11 \le h \le 11$, $-9 \le k \le 11$, $-30 \le l \le 30$
reflections collected	21 322	22 342
independent reflections	4410 [R_{int} = 0.0367, R_{sigma} = 0.0267]	4367 [R_{int} = 0.0271, R_{sigma} = 0.0160]
data/restraints/parameters	4410/1/262	4367/0/244
goodness-of-fit on F^2	1.042	1.061
final R indexes [$I \ge 2\sigma$ (I)]	R_1 = 0.0293, wR_2 = 0.0719	R_1 = 0.0267, wR_2 = 0.0700
final R indexes [all data]	R_1 = 0.0332, wR_2 = 0.0743	R_1 = 0.0291, wR_2 = 0.0722
largest diff. peak and hole (e Å^{-3})	0.21/−0.18	0.50/−0.58
Flack parameter	−0.013 (8)	
CCDC No.	2094457	2094458

structural optimization in the gas phase as described in Section 4. The structural superimposition of the respective X-ray and optimized structures is shown in Figures S9−S12. It clearly shows that a slight structural deviation is observed around the phenyl rings in all four structures, indicating a crystal packing effect. Further, we modeled compounds **1** and **2** in two different conformations (X-ray conformation of compounds **1** and **2**; Figure S13) to obtain the energy difference between the two conformers. The modeling studies suggest that the most stable conformer for both compounds is folded conformation. The nonfolded conformation (X-ray structure of compound **2**) is slightly less stable than the corresponding folded conformation modeled in this study. The energy difference between the folded and nonfolded conformations of **1** is only about 3.9 kcal mol^{-1}, whereas the corresponding value is 3.6 kcal mol^{-1} for compound **2**.

2.3. Hirshfeld Surface Analysis and 2D-Fingerprint Plots. The Hirshfeld surface (HS) analysis has become an invaluable tool for extrapolating additional information about the interactions formed between the molecules in crystals. In Figure 3, we show two different views of the HS over the d_{norm} values for compounds **1** and **2** and the closely related compounds. The intense red spots in this figure point to the presence of an O(lp)···C(π) intermolecular contact (Figure

https://doi.org/10.1021/acsomega.1c03559
ACS Omega 2021, 6, 27026−27037

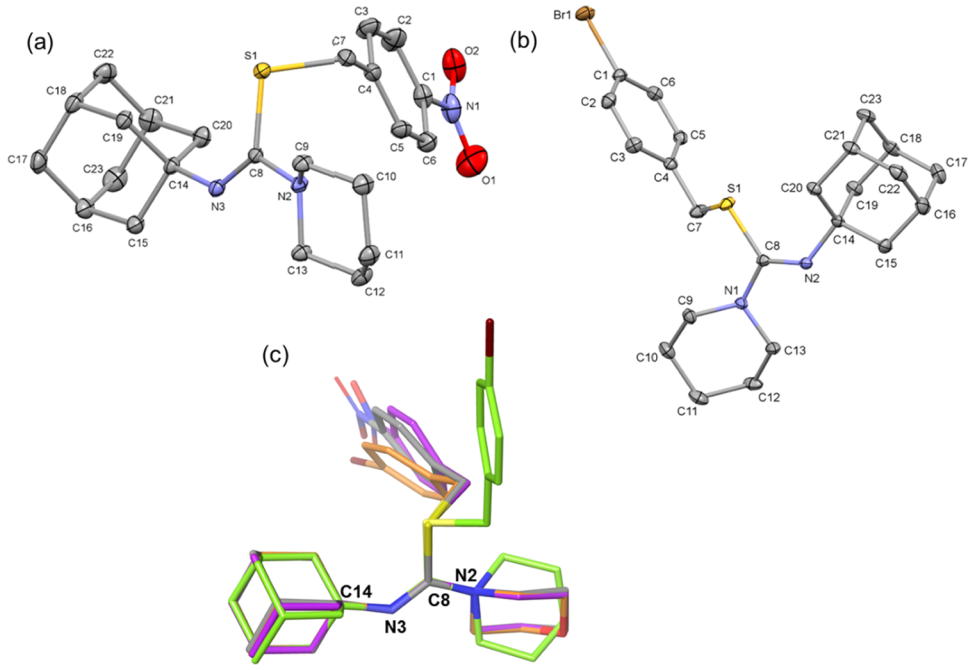

Figure 2. Thermal ellipsoid plots of compounds (a) **1** and (b) **2** are drawn at the 50% probability level, with H atoms omitted for clarity, and (**c**) structural superimposition of structures **1** (gray) and **2** (green) with their closely related structures (REMHID (violet) and KUBDET (orange)) using the labeled atoms.

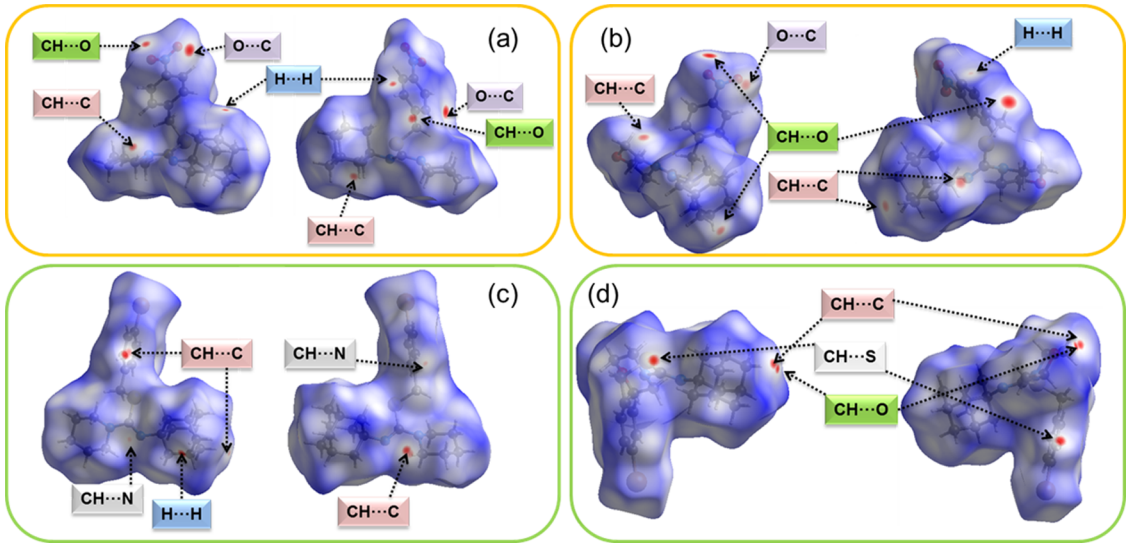

Figure 3. Two different orientations of the Hirshfeld surfaces showing red spots corresponding to the close inter-contacts observed in structures (a) **1** and (b) REMHID, (c) **2** and (d) KUBDET.

3a). It is also possible to see two small red spots on the HS coming from intermolecular C−H···O and C−H···C interactions. For the C−H···O interaction, the oxygen (O1 atom) of the nitro group acts as a proton acceptor. There is a small red spot associated with the short H···H contact. Also, a closely related structure (REMHID) of **1** exhibits a similar feature (Figure 3b).

On the HS of compound **2**, there are small red spots that indicate intermolecular C−H···C and short H···H contacts (Figure 3c). However, a tiny and less intense red spot corresponds to the C−H···N interaction in which the N2 atom has served as an acceptor. Different close contacts are visible on the HS of a closely related structure (KUBDET). In KUBDET, the intermolecular C−H···S/O interactions are visible on the HS in addition to the C−H···C interaction. No C−H···N interaction is found within the sum of the vdw radii of H and N atoms (Figure 3d).

The 2D-fingerprint plots generated from the Hirshfeld surface were used to determine the quantitative contributions of the different inter-contacts in order to understand the effect of morpholine/piperidine and nitro/Br substituents (see Figures S14−S17). In Table 2, we summarize the relative contributions of the various inter-contacts between **1**, **2** and their closely related structures. The intermolecular H···H contacts occupy the majority of the HS area of compounds **1**, **2** and their closely related structures, ranging from 65.5 to 71.7% of the total HS area. In order to determine the impact of piperidine/morpholine substitution, we examined two pairs of

https://doi.org/10.1021/acsomega.1c03559
ACS Omega 2021, 6, 27026−27037

Table 2. Relative Contributions (in %) of Various Intermolecular Contacts among Compounds 1, 2, and Their Closely Related Structures

inter-contacts	compound 1	REMHID	compound 2	KUBDET
H···H	70.5	65.4	71.7	68.5
H···O	17	21.9	0	4.8
H···C	4.3	4	12	5.9
H···Br	0	0	13.1	14
H···S	3.5	3.4	1.9	4.1
C···C	0.5	0.8	0	1.4
N···C	0.9	1.1	0	0
H···N	1.5	1.6	1.2	0.5
C···O	1.6	1.6	0	0

structures, such as **1**−REMHID and **2**−KUBDET. For most inter-contacts, **1** and REMHID contributed similar effects, except for H···H and H···O contacts. As a result of morpholine substitution, the contribution to the former contact is slightly reduced (∼5%), and there is a similar increase in the contribution to the latter contact. This analysis also suggests that morpholine oxygen contributed only 4.9% to crystal packing. In KUBDET, the relative contribution of H···O contacts is similar to REMHID, suggesting that nitro groups contribute more to crystal packing than morpholine oxygen. However, the contribution of H···C contacts is reduced by 6% from the total HS area, which could primarily be attributed to KUBDET's morpholine moiety.

Furthermore, we investigated the influence of nitro/Br substituents on morpholine/piperidine moieties. Despite the presence of piperidine and morpholine, the contribution of intermolecular H···Br interaction is nearly unchanged (13.1% in **2** and 14% in KUBDET). In all four structures, other contacts such as H···S, H···N, and C···O contribute less than 5%. It is important to note that $\pi\cdots\pi$ interaction (C···C) contributes only 1.4% in KUBDET. The red and blue triangles on the shape index plot indicate the presence of this interaction, while the pattern of triangles does not appear in the other three structures (Figure S18). The unconventional inter-contact of the type O(lp)···C(π) contributes only about 1.6% towards the crystal packing of **1** and REMHID. In these two structures, only this contact appears, and in the other two structures, the corresponding contact appears beyond the sum of the vdW radii of C and O atoms.

2.4. Crystal Packing. *2.4.1. Crystal Packing of Compound 1.* The crystal packing of **1** is best described as a columnar packing projected onto the *ab* plane (Figure 4a). In each column, two molecules form an M-shaped arrangement (or a W-shaped arrangement). We also note that the crystal packing of the closely related structure REMHID is very similar to that of compound **1** (Figure S19). Furthermore, the crystal structure of **1** is composed of intermolecular C−H···S, C−H···O, and O(lp)···C(π) interactions. The closely related structure REMHID also depends on C−H···S, C−H···O, and O(lp)···C(π) interactions for stabilization. Besides the nitro group, morpholine oxygen also participates in the intermolecular C−H···O interaction in this structure. The CLP-PIXEL calculation revealed four molecular pairs with intermolecular interaction energies that ranged from −11.0 to −2.6 kcal mol^{-1} in **1** (Table 3), and six molecular dimers with interaction energies ranging from −10.1 to −1.8 kcal mol^{-1} in REMHID (see Table S1). The presence of morpholine oxygen in this structure leads to two additional dimers. The molecular dimers observed in REMHID are shown in Figure S20.

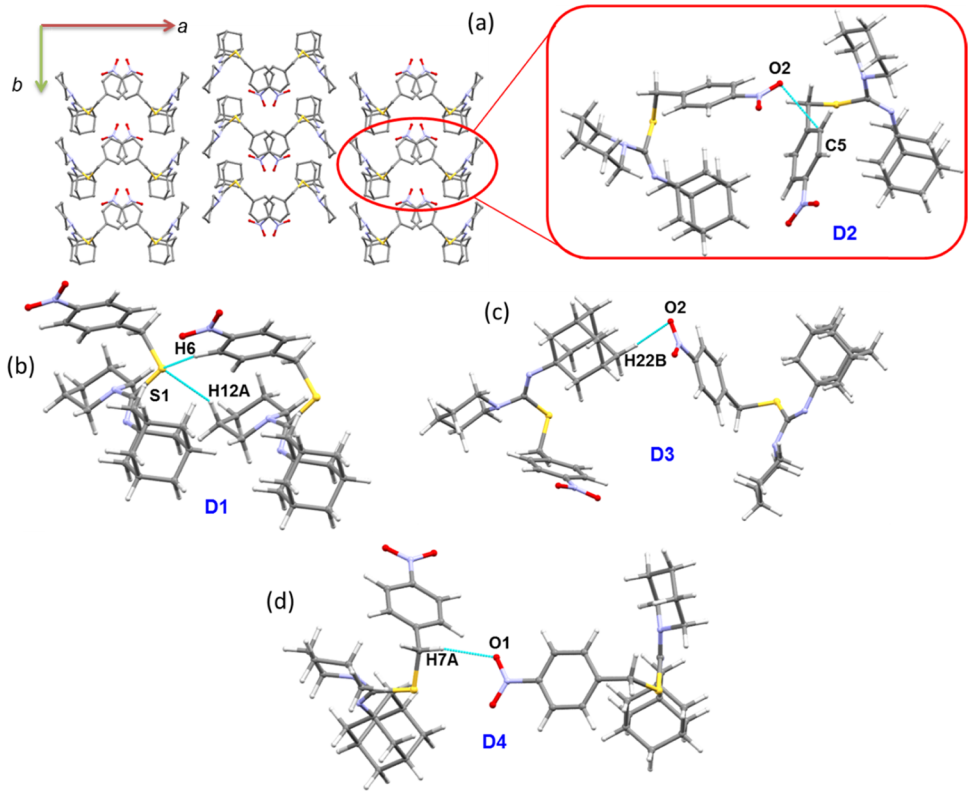

Figure 4. (a) Crystal packing of **1** and its basic structural motif D2 and (b−d) other dimers observed in this structure.

https://doi.org/10.1021/acsomega.1c03559
ACS Omega 2021, 6, 27026−27037

Table 3. Intermolecular Interaction Energies (in kcal mol^{-1}) for Different Dimers Observed in the Crystal Structures of 1 and 2

					PIXEL/MP2/6-31G**					B97D3/def2-TZVP
dimer	CD	symmetry	important interactions	geometry[a] H···A (Å), ∠D−H···A (deg)	E_{Coul}	E_{pol}	E_{disp}	E_{rep}	E_{tot}	ΔE_{cp}
				Compound **1**						
D1	6.794	$x, y-1, z$	C6−H6···S1	2.87, 129	−4.7	−2.7	−16.0	12.4	−11.0	−13.1
			C12−H12A···S1	2.90, 150						
D2	8.437	$-x+1/2, y, z+1/2$	O2(lp)···C5(π)	3.061 (1)	−2.2	−1.3	−7.6	5.4	−5.7	−7.1
D3	10.832	$-x+1/2, y-1, z-1/2$	C22−H22B···O2	2.60, 152	−0.8	−0.5	−3.6	2.1	−2.9	−3.3
D4	10.832	$-x+1/2, y-1, z+1/2$	C7−H7A···O1	2.49, 161	−1.6	−0.5	−1.7	1.2	−2.6	−3.2
				Compound **2**						
D1	5.496	$-x+1, y-1/2, -z+3/2$	C5−H5···N2	2.60, 156	−5.6	−2.8	−20.3	14.4	−14.4	−17.6
D2	9.555	$x-1, y, z$	C11−H11A···C5(π)	2.87, 157	−1.6	−0.6	−7.5	4.6	−5.2	−7.0
D3	12.136	$x, -y+1/2, z+1/2$	C17−H17A···C2(π)	2.72, 156	−1.3	−0.6	−5.6	3.8	−3.7	−5.1
			C22−H22B···C6(π)	2.82, 165						
D4	14.279	$x-1, -y+1/2, z-1/2$	C15−H15A···Br1	3.00, 116	−0.6	−0.3	−2.3	1.6	−1.5	−2.0

[a]Neutron values are given for all D−H···A interactions. CD: distance between the geometrical centers of the molecules.

In compound **1**, a bifurcated intermolecular C−H···S interaction forms the most stable dimer (D1) (Figure 4b). We estimate that this dimer is stabilized by 68% due to its dispersion energy component. The unconventional O···C (lp···π interaction) contact that led to the second most stable dimer (D2) with a distance of 3.061 (1) Å served as a basic structural motif (Figure 4a). Dimer D2 experiences a 68% contribution from dispersion energy, as seen in dimer D1. One of the oxygens (O2) of the nitro moiety is involved as an acceptor for the intermolecular C−H···O interaction in which one of the protons of the adamantane moiety is involved as a donor (H22B). This weak interaction creates the dimer D3 and connects the molecules of **1** into a chain that runs parallel to the c axis (Figure 4c). An analysis of the PIXEL energy shows that the dispersion energy contributes ∼73% to the stabilizing dimer D3. The dimer D4 is stabilized by an intermolecular C−H···O interaction in which the linker methylene interacts with one of the oxygen atoms (O1) of the nitro group (Figure 4d). As a result of this interaction, the molecules form a chain. Compared to the D3 dimer, dimer D4's electrostatic energy component contributes 55% (45% of the dispersion energy) to stabilization. It is important to note that dimers D1, D2, D4, and D5 in REMHID are similar to those in **1**. The D3 and D6 dimers of REMHID are primarily generated through C−H···O interaction involving morpholine oxygen as an acceptor. The former dimer formed a ring with an $R_2^2(8)$ motif, while the latter dimer formed a chain that runs parallel to the crystallographic *c* axis.

In order to gain more insight into the observed intermolecular interactions in **1**, we calculated the molecular electrostatic potential (MESP) map (Figure S21). The most positive electrostatic potentials ($V_{s,max}$) were observed for the protons of the bridge methylene group, phenyl, and piperidine rings compared to the protons of the adamantane moiety. The most negative electrostatic potentials ($V_{s,min}$) were observed for the oxygen atoms of the nitro group (O1: −34.7 kcal mol^{-1} and O2: −34.5 kcal mol^{-1}). These atoms were likely to interact with the positive ESP regions of the protons (H7A: 25.5 kcal mol^{-1} and H22B: 7.4 kcal mol^{-1}). Similarly, the negative ESP was observed near the S atom with the $V_{s,min}$ value of −10.0 kcal mol^{-1}, and this atom is involved in a bifurcated interaction with the positive ESP regions of atoms H6 (19.8 kcal mol^{-1}) and H12A (20.7 kcal mol^{-1}). The observed O2···C5 (lp···π interaction) contact was further examined with the MESP. The π-hole was observed near atom C5 with a $V_{s,max}$ value of 0.8 kcal mol^{-1} and interacts with the lone pair of atom O2.

An energy framework has been constructed that visualizes the crystal packing of compound **1**, which comprises the intermolecular interaction energies between different molecular pairs. Figure 5 illustrates the structure of the energy framework as ladder-like, with horizontal and diagonal tubes connecting adjacent ladders. A similar topology has also been observed in the crystal structure of (*Z*)-3-(adamantan-1-yl)-*S*-(4-bromobenzyl)-1-(3-chlorophenyl)isothiourea[30] and in the closely related structure REMHID, as expected. In the ladder, the large vertical tubes correspond to intermolecular C−H···S

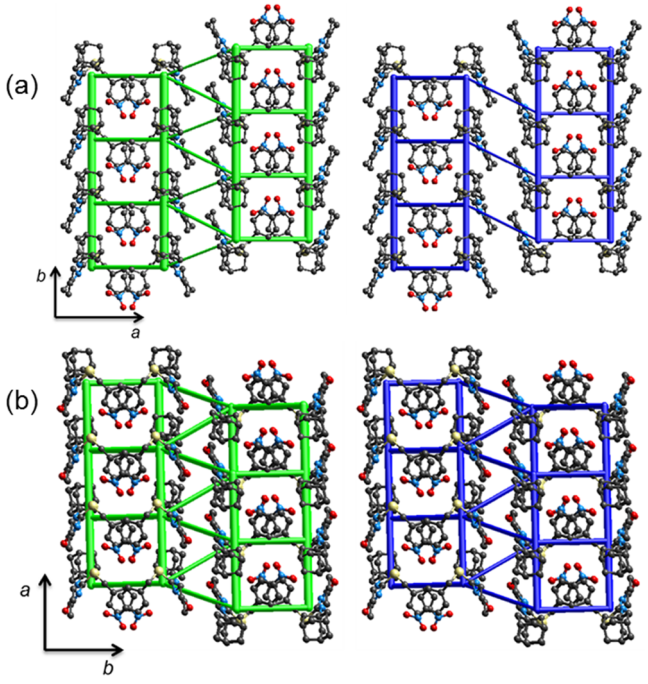

Figure 5. Energy frameworks for the crystal structure of (a) **1** and (b) REMHID. The dispersion (green) and net interaction (blue) energies are represented as cylindrical tubes with the size 80. The interaction energies with magnitudes smaller than −15 kJ mol^{-1} have been omitted for clarity.

https://doi.org/10.1021/acsomega.1c03559
ACS Omega 2021, 6, 27026−27037

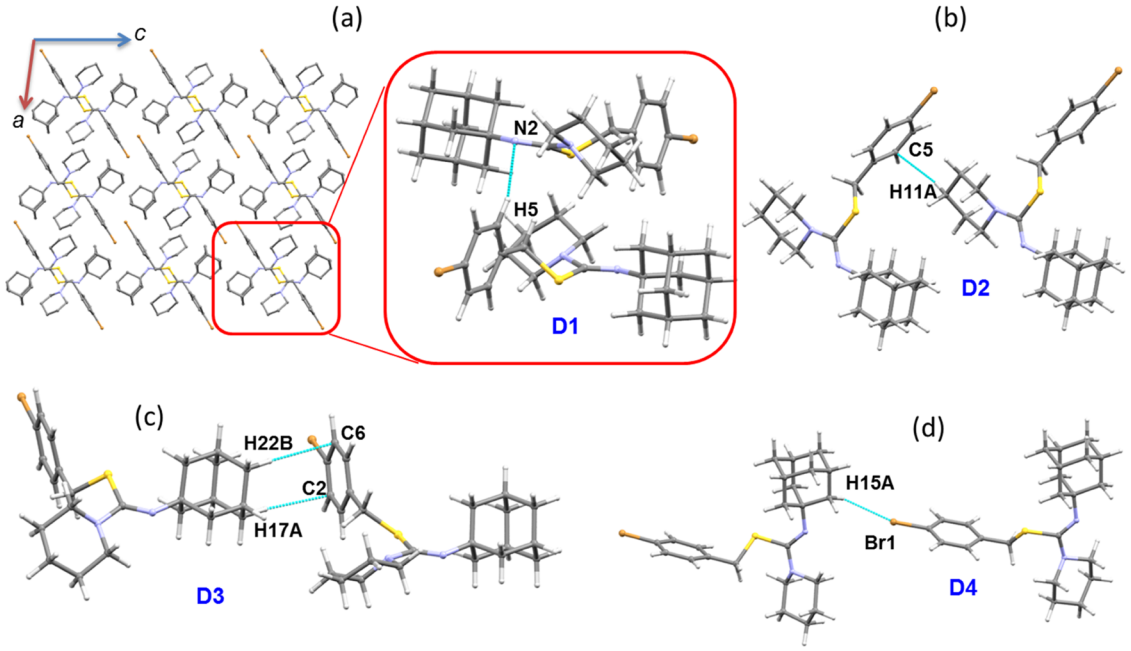

Figure 6. (a) Crystal packing of compound **2** and its basic structural motif (D1) are highlighted; (b–d) different molecular pairs (D2–D4) held together with different types of noncovalent interactions.

interactions, and the smaller horizontal cylindrical tubes to C–H···O interactions and O(lp)···C(π) contacts. The zigzag tube connects the two adjacent ladders primarily through H···H contacts between piperidine–adamantyl and piperidine–piperidine moieties. In the crystal structure of compound **1**, the diameter of the cylindrical tubes for dispersion and the total interaction energies are comparable, which suggests that the dispersion energy component is predominant in the interaction energies of the molecular pairs. As expected, the energy framework for the crystal packing in REMHID is very similar to that of compound **1**. However, the ladder-like arrangement in REMHID runs parallel to the crystallographic *a* axis rather than the *b* axis.

2.4.2. Crystal Packing of Compound 2. The crystal packing of compound **2** can also be projected onto the *ac* plane in a columnar fashion (Figure 6a). The basic structural motif is stabilized by an intermolecular C–H···N interaction (involving H5 and N2 atoms), and this interaction may also stabilize the *anti*-periplanar conformation of the molecule **2**. The PIXEL calculation revealed that the basic structural motif forms the most stable dimer (D1), with the intermolecular interaction energy of −14.4 kcal mol^{-1}. As this dimer and the other three dimers formed in this structure are dispersive, the dispersion energy contributes more than 70% to stabilize them. The intermolecular interaction between the piperidine ring proton (H11A) and the phenyl ring atom C5 leads to a further potent dimer (D2) (Figure 6b) with an intermolecular interaction energy value of −5.2 kcal mol^{-1}. This weak interaction links the neighboring molecules and creates a chain parallel to the crystallographic *a* axis. Dimer D3 demonstrates two C–H···C interactions between adamantane and the carbon atoms of the phenyl ring (Figure 6c).

These weak interactions link the neighboring molecules into a chain that runs parallel to the crystallographic *c* axis. Among the dimers, the least stable dimer (D4) is formed by an intermolecular C–H···Br interaction that interconnects the adjacent molecules into a chain (Figure 6d).

In the MESP map for compound **2** (Figure S21), the most positive electrostatic potentials ($V_{s,max}$) are observed in the order (benzene > piperidine > adamantane) for hydrogens associated with these moieties. The observed C–H···N interaction can be explained with the MESP map. The positive and negative ESP were observed near atoms H5 (17.8 kcal mol^{-1}) and N2 (−30.7 kcal mol^{-1}). These two atoms were likely to participate in noncovalent bonding. The MESP map also reveals the σ-hole at the tip of the C–Br bond with the $V_{s,max}$ value of 10.6 kcal mol^{-1} and a characteristic negative belt around the Br atom ($V_{s,min}$: −12.2 to −11.5 kcal mol^{-1}).

Although KUBDET is very similar to compound **2**, KUBDET uses different types of intermolecular interactions for stabilization compared to **2**. The molecules of KUBDET were packed in a columnar fashion (Figure S22) and five potential dimers were formed in the solid state (Table S2 and Figure S23). The intermolecular interaction energies for these dimers range from −10.6 to −1.9 kcal mol^{-1}. These five dimers are stabilized by intermolecular C–H···S, C–H···O, C–H···Br, and π···π interactions. The dimer D1 (E_{tot}: −10.6 kcal mol^{-1}) is formed by a bifurcated C–H···S interaction, which is very similar to the dimer D1 in compound **1** and REMHID. These structures have similar intermolecular interaction energies for this dimer. In KUBDET, the second most stable dimer, D2, is formed by a π-stacking interaction between the molecules related to the center of inversion. The other three structures do not form this stacking interaction. In this structure, a pair of intermolecular C–H···Br interactions form a centrosymmetric dimer D3, whereas the corresponding interaction generates a chain in **2**. The former dimer is relatively strong as it forms a centrosymmetric dimeric motif, whereas the latter dimer is relatively weak as it generates a chain motif. The dimers D4 and D5 are formed by intermolecular C–H···O interactions in which morpholine oxygen is involved as an acceptor. Dimer D4 is a centrosymmetric dimer that is similar to dimer D3 in REMHID, and their interaction energies are similar. We also

https://doi.org/10.1021/acsomega.1c03559
ACS Omega 2021, 6, 27026−27037

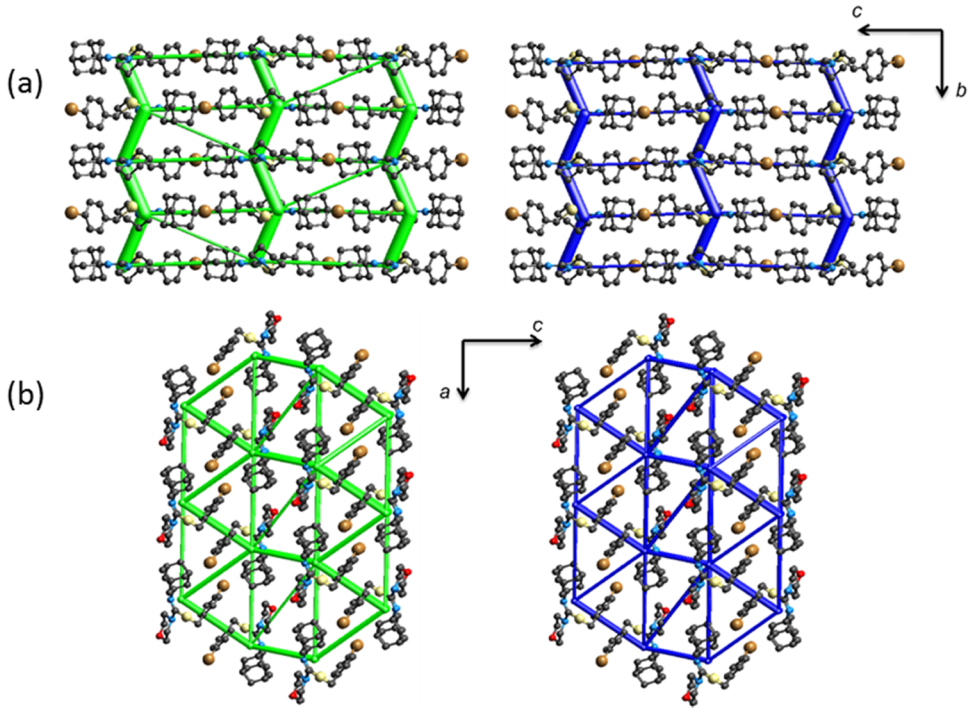

Figure 7. Energy frameworks for the crystal structure of (a) **2** and (b) KUBDET. The dispersion (green) and net interaction (blue) energies are represented as cylindrical tubes with the size 80. The interaction energies with magnitudes smaller than −15 kJ mol^{-1} have been omitted for clarity.

note that dimer D5 of KUBDET and dimer D6 of REMHID are similar and their interaction energies are comparable.

Further, we visualized the crystal packing through pairwise interaction energies. An energy framework is shown for the crystal structure of compound **2** along the crystallographic *a* axis (Figure 7a). We observe that structures **1** and **2** have different topologies for their energy frameworks. In this structure, the intermolecular C−H···N interaction is represented by the vertical, zigzag cylindrical tubes. This interaction helps to form the basic structural motif. The larger zigzag cylindrical tubes also represent the columnar packing. It is interesting to note that the adjacent zigzag tubes have been interconnected with smaller horizontal and diagonal tubes. These two smaller tubes correspond to intermolecular C−H···C interactions. The diameters of the cylindrical tubes for dispersion and total interaction energies are comparable, indicating that the dispersion energy component is predominant in the interaction energies of the molecular pairs in compound **2**. The energy frameworks for the crystal structure of KUBDET are somewhat similar to those of **1** and REMHID and different from those of compound **2** (Figure 7b). The 3D-topology of the KUBDET is primarily constructed by intermolecular C−H···S, C−H···O, and C−H···Br interactions. As observed in the other three structures, the energy frameworks are predominantly dispersive in nature, as evident from the diameter of the cylindrical tubes.

2.5. Molecular Docking Analysis. The in vitro antiproliferative activity of compounds **1** and **2** was evaluated against HL-60 (human promyelocytic leukemia cell line), HT-29 (human colorectal cancer cell line), and MCF7 (human breast cancer cell line) by MTT assay (Table S4).[26] As compared with the potent anticancer drug Doxorubicin, compounds **1** and **2** showed optimal activity with IC_{50} < 10 μM against these cell lines. Molecular docking analysis was used to determine the possible binding modes of compounds **1** and **2** at the active site of the human sphingosine kinase 1 (SPHK1) protein, using the Glide XP docking scoring scheme implemented in the Schrodinger suite. Both compounds (**1**: −9.384 kcal mol^{-1} and **2**: −9.047 kcal mol^{-1}) showed similar glide XP scores, which are in good agreement with the observations of antiproliferative in vitro activity. The bound conformation of compounds **1** and **2** adopts a nonfolded conformation that is similar to the X-ray conformation of **2**. As shown in Figure 8, these two compounds occupy the position of the known SPHK1 inhibitor [(2*R*)-1-[[(4-[[3-methyl-5-[(phenylsulfonyl)methyl]phenoxy]methyl]phenyl]methyl]-2-pyrrolidinemethanol] (PF-543),[50] which is bound at the lipid-binding site closer to the ATP site. The piperidine and adamantyl moieties of compounds **1** and **2** are positioned near

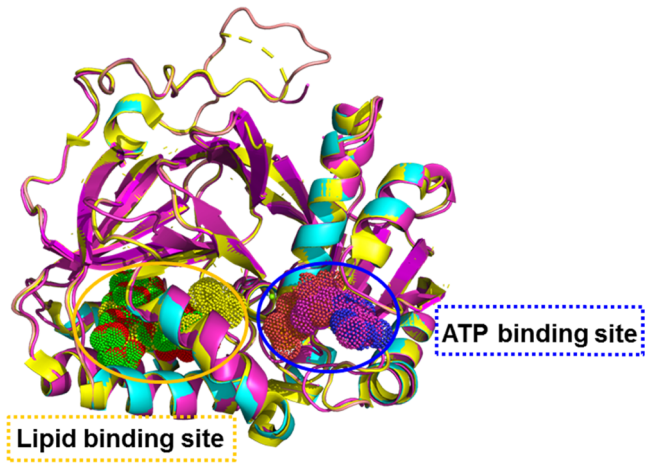

Figure 8. Compounds **1** (green dots) and **2** (red dots) bound at the lipid-binding site of the SPHK1 protein. The known inhibitor PF-543 is shown in dots (yellow) representation.

https://doi.org/10.1021/acsomega.1c03559
ACS Omega 2021, 6, 27026−27037

hydrophobic residues in the lipid-binding pocket. The 2D ligand−protein interaction diagrams are shown in Figures S26 and S27. We can see from the figures that the nitro group of compound **1** has participated in the cation−π interaction with the Phe 278 residue in addition to hydrophobic interactions. Compound **2** makes only hydrophobic interactions with the residues at the active site. Overall, the docking analysis indicates that compounds **1** and **2** have the ability to bind to the lipid-binding site of the SPHK1, and the hydrophobic interactions help to form a molecular complex.

3. CONCLUSIONS

Two new adamantyl derivatives with 4-nitrophenyl and 4-bromophenyl functionalities have been synthesized and characterized through single-crystal X-ray diffraction techniques. The crystal structures of these compounds were compared with the structures of their closely related morpholine analogs REMHID and KUBDET. A comparative analysis of the structures revealed that compound **2** shows *anti*-periplanar conformation and the other three structures show *syn*-clinal conformation. Hirshfeld surface analysis showed that the morpholine substitution reduces the H···H interaction and slightly increases the H···O interaction in compounds with the nitro group. Moreover, the morpholine oxygen contributes less compared to the nitro oxygen as an acceptor toward crystal packing. On the other hand, the morpholine substitution reduces the contribution of H···H interaction and reduces the H···C/O interactions in compounds containing the Br substituent. The contribution of the H···Br contact is nearly the same in both piperidine- and morpholine-containing derivatives. The CLP-PIXEL energy analysis revealed various molecular pairs held by different intermolecular interactions in all four structures. Compound **1** is stabilized by bifurcated C−H···S, C−H···O, and unconventional O···C contacts, and the basic structural unit was found to be stabilized by the O···C contact. In contrast, compound **2** is stabilized by C−H···N, C−H···C, and C−H···Br interactions, of which the C−H···N interaction generates the basic structural unit. We observed that the crystal structures of **1** and its closely related structure REMHID share similar molecular dimers and similar energy frameworks. Compound **2** and its closely related structure KUBDET display columnar packing, but the interactions that stabilize the molecular dimers are different. The latter structure has a bifurcated C−H···S and π-stacking interaction, which are not present in **2**. The in silico molecular docking analysis supported the binding potential of the title compounds against the SPHK1 enzyme.

4. MATERIALS AND METHODS

4.1. Synthesis and crystallization. Compounds **1** and **2** were synthesized following the reaction sequences outlined in Scheme 1.[26,49] Pure single crystals for X-ray diffraction were obtained by slow evaporation of a solution of the compounds in EtOH/$CHCl_3$ (1:1, v/v) at room temperature.

*4.1.1. 4-Nitrobenzyl N′-(adamantan-1-yl)piperidine-1-carbothioimidate (**1**).* Colorless plate crystals; M.P. 116−118 °C; mol. formula (mol. wt.): $C_{23}H_{31}N_3O_2S$ (413.58).

*4.1.2. 4-Bromobenzyl N′-(adamantan-1-yl)piperidine-1-carbothioimidate (**2**).* Colorless plate crystals; M.P. 96−98 °C; mol. formula (mol. wt.): $C_{23}H_{31}BrN_2S$ (447.47).

4.2. Single-Crystal X-ray Diffraction Determination. Single-crystal X-ray diffraction data were collected for crystals **1** and **2** at 160 (1) K on a Rigaku OD SuperNova/Atlas area-detector diffractometer using Cu Kα radiation (λ = 1.54184 Å) from a microfocus X-ray source and an Oxford Instruments Cryojet XL cooler. The selected suitable single crystal was mounted using polybutene oil on a flexible loop fixed on a goniometer head and immediately transferred to the diffractometer. Pre-experiment, data collection, data reduction, and analytical absorption correction[51] were performed with the program suite *CrysAlisPro*, version 1.171.40.68a (Rigaku Oxford Diffraction, England, 2019). Using *Olex2*,[52] the structure was solved with the SHELXT[53] small-molecule structure solution program and refined with the *SHELXL2018/3* program package[54] by full-matrix least-squares minimization on F^2. All of the H atoms were placed in calculated positions (C−H = 0.95−1.00 Å) and were constrained to ride on their parent atoms, with U_{iso}(H) = 1.2U_{eq}(C). The *PLATON* program was used to check the result of the X-ray analysis.[55] The crystal packing and molecular dimers were drawn using the program MERCURY.[56]

4.3. Theoretical Calculations. For all calculations, we used the crystal structure geometry with the normalized H positions (C−H = 1.083 Å). Energy framework analysis[57,58] was performed using the CrystalExplorer-17.5 program[59] with the B3LYP/6-31G(d,p) level of approximation. The Hirshfeld surface[43] and 2D-fingerprint plots[44] were obtained from the CrystalExplorer-17.5 program. We calculated the intermolecular interaction energies (E_{tot}) between molecular pairs using the CLP-PIXEL program.[46,60] For this computation, the electron density was obtained with the Gaussian 09 program[61] using the MP2/6-31G** levels of theory. Furthermore, the accurate complexation energies of molecular pairs identified from the CLP-PIXEL energy calculation were calculated using the B97D3/def2-TZVP level of theory, and then, these complexation energies were corrected (ΔE_{cp}) for the basis set superposition error using the counterpoise method.[62] The topological analysis of selected dimers was performed within the framework of Bader's quantum theory of atoms-in-molecules approach (QTAIM) using the AIMALL program.[63] The wave functions were computed at the M062X-D3/cc-pVTZ level of theory for topological analysis. Using the Gaussian program with the M062X-D3/cc-pVTZ level of theory, single-point energy calculations and structural optimization in the gas phase were carried out on compounds **1** and **2** and their closely related structures REMHID and KUBDET. Vibrational frequency calculation confirmed the absence of negative frequency for optimized structures.

Molecular docking analysis was performed with Schrödinger suite 2019-4 (Schrödinger, LLC, New York, NY, 2019). The 3D structure of human sphingosine kinase 1 (SPHK1) was used as a target protein (PDB ID: 4V24) and prepared for docking as described earlier.[30] The location of the inhibitor PF-543 (PDB ligand ID: GYR) molecule was used to generate the receptor grid box. The compounds (**1** and **2**) were prepared for molecular docking using the LIGPREP module with an OPLS3e force field. The glide extra precision (XP) scoring scheme was used to predict the binding modes of the ligand molecules at the active site of the target protein molecule.

https://doi.org/10.1021/acsomega.1c03559
ACS Omega 2021, 6, 27026−27037

■ ASSOCIATED CONTENT

Supporting Information

The Supporting Information is available free of charge at https://pubs.acs.org/doi/10.1021/acsomega.1c03559.

^{1}H and ^{13}C NMR spectra, 2D-fingerprint plots, shape index plots, intermolecular interaction energies for dimers of REMHID and KUBDET, PIXEL energy analysis, crystal packing and dimers of REMHID and KUBDET, the molecular graphs of dimers of **1** and **2** showing bond critical points for intermolecular interactions, and protein−ligand interaction plots (PDF)

■ AUTHOR INFORMATION

Corresponding Author

Subbiah Thamotharan − *Biomolecular Crystallography Laboratory, Department of Bioinformatics, School of Chemical and Biotechnology, SASTRA Deemed University, Thanjavur 613401, India;* orcid.org/0000-0003-2758-6649; Email: thamu@scbt.sastra.edu

Authors

Aamal A. Al-Mutairi − *Department of Chemistry, College of Sciences, Imam Mohammad Ibn Saud Islamic University (IMSIU), Riyadh 11623, Saudi Arabia*

Kowsalya Alagappan − *Biomolecular Crystallography Laboratory, Department of Bioinformatics, School of Chemical and Biotechnology, SASTRA Deemed University, Thanjavur 613401, India*

Olivier Blacque − *Department of Chemistry, University of Zurich, 8057 Zurich, Switzerland*

Monirah A. Al-Alshaikh − *Department of Chemistry, College of Sciences, King Saud University, Riyadh 11451, Saudi Arabia*

Ali A. El-Emam − *Department of Medicinal Chemistry, Faculty of Pharmacy, Mansoura University, Mansoura 35516, Egypt;* orcid.org/0000-0002-9325-9497

M. Judith Percino − *Unidad de Polímeros y Electrónica Orgánica, Instituto de Ciencias, Benemérita Universidad Autónoma de Puebla, Puebla C.P.72960, Mexico;* orcid.org/0000-0003-1610-7155

Complete contact information is available at: https://pubs.acs.org/10.1021/acsomega.1c03559

Notes

The authors declare no competing financial interest.

■ ACKNOWLEDGMENTS

The authors acknowledge SASTRA Deemed to be University for Schrodinger software support. S.T. and M.J.P. would like to thank the Laboratorio Nacional de Supercomputo del Sureste (LNS-BUAP) for computational resources.

■ REFERENCES

(1) Lamoureux, G.; Artavia, G. Use of the adamantane structure in medicinal chemistry. *Curr. Med. Chem.* **2010**, *17*, 2967−2978.

(2) Liu, J.; Obando, D.; Liao, V.; Lifa, T.; Codd, R. The many faces of the adamantyl group in drug design. *Eur. J. Med. Chem.* **2011**, *46*, 1949−1963.

(3) Wanka, L.; Iqbal, K.; Schreiner, P. R. The lipophilic bullet hits the targets: Medicinal chemistry of adamantane derivatives. *Chem. Rev.* **2013**, *113*, 3516−3604.

(4) Spilovska, K.; Zemek, F.; Korabecny, J.; Nepovimova, E.; Soukup, O.; Windisch, M.; Kuca, K. Adamantane - a lead structure for drugs in clinical practice. *Curr. Med. Chem.* **2016**, *23*, 3245−3266.

(5) Davies, W. L.; Grunnert, R. R.; Haff, R. F.; McGahen, J. W.; Neumeyer, E. M.; Paulshock, M.; Watts, J. C.; Wood, T. R.; Hermann, E. C.; Hoffmann, C. E. Antiviral activity of 1-adamantamine (amantadine). *Science* **1964**, *144*, 862−863.

(6) Wendel, H. A.; Snyder, M. T.; Pell, S. Trial of amantadine in epidemic influenza. *Clin. Pharmacol. Ther.* **1966**, *7*, 38−43.

(7) Wingfield, W. L.; Pollack, D.; Grunert, R. R. Treatment of influenza. The therapeutic efficacy of rimantadine HCl in a naturally occurring influenza A_2 respiratory illness in man. *N. Engl. J. Med.* **1969**, *281*, 579−584.

(8) Rosenthal, K. S.; Sokol, M. S.; Ingram, R. L.; Subramanian, R.; Fort, R. C. Tromantadine: Inhibitor of early and late events in *herpes simplex* virus replication. *Antimicrob. Agents Chemother.* **1982**, *22*, 1031−1036.

(9) Long, J.; Manchandia, T.; Ban, K.; Gao, S.; Miller, C.; Chandra, J. Adaphostin cytoxicity in glioblastoma cells is ROS-dependent and is accompanied by upregulation of heme oxygenase-1. *Cancer Chemother. Pharmacol.* **2007**, *59*, 527−735.

(10) Han, T.; Goralski, M.; Capota, E.; Padrick, S. B.; Kim, J.; Xie, Y.; Nijhawan, D. The antitumor toxin CD437 is a direct inhibitor of DNA polymerase α. *Nat. Chem. Biol.* **2016**, *12*, 511−515.

(11) Lorenzo, P.; Alvarez, R.; Ortiz, M. A.; Alvarez, S.; Piedrafita, F. J.; de Lera, A. R. Inhibition of IκB kinase-β and anticancer activities of novel chalcone adamantyl arotinoids. *J. Med. Chem.* **2008**, *51*, 5431−5440.

(12) Dai, L.; Smith, C. D.; Foroozesh, M.; Miele, L.; Qin, Z. The sphingosine kinase 2 inhibitor ABC294640 displays anti-non-small cell lung cancer activities *in vitro* and *in vivo*. *Int. J. Cancer* **2018**, *142*, 2153−2162.

(13) Kurd, R.; Ben-Chetrit, E.; Karameh, H.; Bar-Meir, M. Compassionate use of opaganib for patients with severe COVID-19. *J. Emerg. Dis. Virol.* **2020**, *5* (3), 1−3.

(14) Protopopova, M.; Hanrahan, C.; Nikonenko, B.; Samala, R.; Chen, P.; Gearhart, J.; Einck, L.; Nacy, C. A. Identification of a new antitubercular drug candidate, SQ109, from a combinatorial library of 1,2-ethylenediamines. *J. Antimicrob. Chemother.* **2005**, *56*, 968−974.

(15) Bogatcheva, E.; Hanrahan, C.; Chen, P.; Gearhart, J.; Sacksteder, K.; Einck, L.; Nacy, C.; Protopopova, M. Discovery of dipiperidines as new antitubercular agents. *Bioorg. Med. Chem. Lett.* **2010**, *20*, 201−205.

(16) Hu, H.; Lin, C.; Ao, M.; Ji, Y.; Tang, B.; Zhou, X.; Fang, M.; Zeng, J.; Wu, Z. Synthesis and biological evaluation of 1-(2-(adamantane-1-yl)-1*H*-indol-5-yl)-3-substituted urea/thiourea derivatives as anticancer agents. *RSC Adv.* **2017**, *7*, 51640−51651.

(17) Huang, X.; Huang, R.; Liao, Z.; Pan, Y.; Gou, S.; Wang, H. Synthesis and pharmacological evaluation of dehydroabietic acid thiourea derivatives containing bisphosphonate moiety as an inducer of apoptosis. *Eur. J. Med. Chem.* **2016**, *108*, 381−391.

(18) D'Cruz, O. J.; Uckun, F. M. Novel broad-spectrum thiourea non-nucleoside inhibitors for the prevention of mucosal HIV transmission. *Curr. HIV Res.* **2006**, *4*, 329−345.

(19) Kang, I. J.; Wang, L. W.; Hsu, S. J.; Lee, C. C.; Lee, Y. C.; Wu, Y. S.; Yueh, A.; Wang, J. C.; Hsu, T. A.; Chao, Y. S.; Chern, J. H. Design and efficient synthesis of novel arylthiourea derivatives as potent hepatitis C virus inhibitors. *Bioorg. Med. Chem. Lett.* **2009**, *19*, 6063−6068.

(20) Joshi, S. D.; Dixit, S. R.; Kirankumar, M. N.; Aminabhavi, T. M.; Raju, K. V.; Narayan, R.; Lherbet, C.; Yang, K. S. Synthesis, antimycobacterial screening and ligand-based molecular docking studies on novel pyrrole derivatives bearing pyrazoline, isoxazole and phenyl thiourea moieties. *Eur. J. Med. Chem.* **2016**, *107*, 133−152.

(21) Verlinden, B. K.; Niemand, J.; Snyman, J.; Sharma, S. K.; Beattie, R. J.; Woster, P. M.; Birkholtz, L. M. Discovery of novel alkylated (bis)urea and (bis)thiourea polyamine analogues with potent antimalarial activities. *J. Med. Chem.* **2011**, *54*, 6624−6633.

(22) El-Emam, A. A.; Al-Deeb, O. A.; Al-Omar, M.; Lehmann, J. Synthesis, antimicrobial, and anti-HIV-1 activity of certain 5-(1-adamantyl)-2-substituted thio-1,3,4-oxadiazoles and 5-(1-adamantyl)-3-substituted aminomethyl-1,3,4-oxadiazoline-2-thiones. *Bioorg. Med. Chem.* **2004**, *12*, 5107−5113.
(23) El-Emam, A. A.; Al-Tamimi, A. M. S.; Al-Omar, M. A.; Alrashood, K. A.; Habib, E. E. Synthesis and antimicrobial activity of novel 5-(1-adamantyl)-2-aminomethyl-4-substituted-1,2,4-triazoline-3-thiones. *Eur. J. Med. Chem.* **2013**, *68*, 96−102.
(24) Al-Wahaibi, L. H.; Hassan, H. M.; Abo-Kamar, A. M.; Ghabbour, H. A.; El-Emam, A. A. Adamantane-isothiourea hybrid derivatives: synthesis, characterization, *in vitro* antimicrobial, and *in vivo* hypoglycemic activities. *Molecules* **2017**, *22*, No. 710.
(25) Hassan, H. M.; Al-Wahaibi, L. H.; Shehatou, G. S.; El-Emam, A. A. Adamantane-linked isothiourea derivatives suppress the growth of experimental hepatocellular carcinoma via inhibition of TLR4-MyD88-NF-κB signaling. *Am. J. Cancer Res.* **2021**, *11*, 350−369.
(26) Al-Mutairi, A. A.; Al-Alshaikh, M. A.; Al-Omary, F. A. M.; Hassan, H. M.; El-Mahdy, A. M.; El-Emam, A. A. Synthesis, antimicrobial, and anti-proliferative activities of novel 4-(adamantan-1-yl)-1-arylidene-3-thiosemicarbazides, 4-arylmethyl *N*′-(adamantan-1-yl)piperidine-1-carbothioimidates, and related derivatives. *Molecules* **2019**, *24*, No. 4308.
(27) Al-Wahaibi, L. H.; Joubert, J.; Blacque, O.; Al-Shaalan, N. H.; El-Emam, A. A. Crystal structure, Hirshfeld surface analysis and DFT studies of 5-(adamantan-1-yl)-3-[(4-chlorobenzyl)sulfanyl]-4-methyl-4*H*-1,2,4-triazole, a potential 11β-HSD1 inhibitor. *Sci. Rep.* **2019**, *9*, No. 19745.
(28) Al-Wahaibi, L. H.; Grandhi, D. S.; Tawfik, S. S.; Al-Shaalan, N. H.; Elmorsy, M. A.; El-Emam, A. A.; Percino, M. J.; Thamotharan, S. Probing the effect of halogen substituents (Br, Cl, and F) on the non-covalent interactions in 1-(adamantan-1-yl)-3-arylthiourea derivatives: A Theoretical Study. *ACS Omega* **2021**, *6*, 4816−4830.
(29) El-Emam, A. A.; Saveeth Kumar, E.; Janani, K.; Al-Wahaibi, L. H.; Blacque, O.; El-Awady, M. I.; Al-Shaalan, N. H.; Percino, M. J.; Thamotharan, S. Quantitative assessment of the nature of non-covalent interactions in *N*-substituted-5-(adamantan-1-yl)-1,3,4-thiadiazole-2-amines: Insights from crystallographic and QTAIM analysis. *RSC Adv.* **2020**, *10*, 9840−9853.
(30) Al-Omary, F. A. M.; Chowdary Gude, N.; Al-Rasheed, L. S.; Alkahtani, H. N.; Hassan, H. M.; Al-Abdullah, E. S.; El-Emam, A. A.; Percino, M. J.; Thamotharan, S. X-Ray and theoretical investigation of (*Z*)-3-(adamantan-1-yl)-1-(phenyl or 3-chlorophenyl)-*S*-(4-bromobenzyl)isothioureas: An exploration involving weak non-covalent interactions, chemotherapeutic activities and QM/MM binding energy. *J. Biomol. Struct. Dyn.* **2020**, DOI: 10.1080/07391102.2020.1840443.
(31) Al-Wahaibi, L. H.; Sujay, S.; Muthu, G. G.; El-Emam, A. A.; Venkataramanan, N. S.; Al-Omary, F. A. M.; Ghabbour, H. A.; Percino, J.; Thamotharan, S. Theoretical investigations of two adamantane derivatives: A combined X-Ray, DFT, QTAIM analysis and molecular docking. *J. Mol. Struct.* **2018**, *1159*, 233−245.
(32) Saeed, A.; Erben, M. F.; Bolte, M. Synthesis, Structural and Vibrational Properties of 1-(Adamantane-1-Carbonyl)-3-Halophenyl Thioureas. *Spectrochim. Acta, Part A* **2013**, *102*, 408−413.
(33) Arshad, N.; Saeed, A.; Perveen, F.; Ujan, R.; Farooqi, S. I.; Ali Channar, P.; Shabir, G.; El-Seedi, H. R.; Javed, A.; Yamin, M.; Bolte, M.; Hökelek, T. Synthesis, X-Ray, Hirshfeld Surface Analysis, Exploration of DNA Binding, Urease Enzyme Inhibition and Anticancer Activities of Novel Adamantane-Naphthyl Thiourea Conjugate. *Bioorg. Chem.* **2021**, *109*, No. 104707.
(34) Steiner, T.; R Desiraju, G. Distinction between the Weak Hydrogen Bond and the van Der Waals Interaction. *Chem. Commun.* **1998**, *No. 8*, 891−892.
(35) Ghosh, S.; Chopra, P.; Wategaonkar, S. C−H···S Interaction Exhibits All the Characteristics of Conventional Hydrogen Bonds. *Phys. Chem. Chem. Phys.* **2020**, *22*, 17482−17493.
(36) Bosch, E. Role of Sp-C−H—N Hydrogen Bonding in Crystal Engineering. *Cryst. Growth Des.* **2010**, *10*, 3808−3813.
(37) Salonen, L. M.; Ellermann, M.; Diederich, F. Aromatic Rings in Chemical and Biological Recognition: Energetics and Structures. *Angew. Chem., Int. Ed.* **2011**, *50*, 4808−4842.
(38) Nishio, M. The CH/π Hydrogen Bond in Chemistry. Conformation, Supramolecules, Optical Resolution and Interactions Involving Carbohydrates. *Phys. Chem. Chem. Phys.* **2011**, *13*, 13873−13900.
(39) Safin, D. A.; Babashkina, M. G.; Robeyns, K.; Garcia, Y. C−H···Br−C vs. C−Br···Br−C vs. C−Br···N Bonding in Molecular Self-Assembly of Pyridine-Containing Dyes. *RSC Adv.* **2016**, *6*, 53669−53678.
(40) Sharma, K.; Mohan, T. P.; Gangwar, U.; Chopra, D. Role of Lone Pair- π Interaction and Halogen Bonding in the Crystal Packing of 1,2,4-Oxadiazole Derivatives. *J. Mol. Struct.* **2019**, *1197*, 742−752.
(41) Mooibroek, T. J.; Gamez, P.; Reedijk, J. Lone Pair−π Interactions: A New Supramolecular Bond? *CrystEngComm* **2008**, *10*, 1501−1515.
(42) Al-Ghulikah, H. A.; Ghabbour, H. A.; Tiekink, E. R. T.; El-Emam, A. A. Crystal structure of 4-bromobenzyl (*Z*)-*N*-(adamantan-1-yl)morpholine-4-carbothioimidate, $C_{22}H_{29}BrN_2OS$. *Z. Kristallogr.* **2019**, *234*, 1001−1003.
(43) Spackman, M. A.; Jayatilaka, D. Hirshfeld surface analysis. *CrystEngComm* **2009**, *11*, 19−32.
(44) Spackman, M. A.; McKinnon, J. J. Fingerprinting intermolecular interactions in molecular crystals. *CrystEngComm* **2002**, *4*, 378−392.
(45) Gavezzotti, A. Calculation of intermolecular interaction energies by direct numerical integration over electron densities. I. Electrostatic and polarization energies in molecular crystals. *J. Phys. Chem. B* **2002**, *106*, 4145−4154.
(46) Gavezzotti, A. Calculation of intermolecular interaction energies by direct numerical integration over electron densities. 2. An improved polarization model and the evaluation of dispersion and repulsion energies. *J. Phys. Chem. B* **2003**, *107*, 2344−2353.
(47) Bader, R. F. W. *Atoms in Molecules: A Quantum Theory*; Oxford University Press: USA, 1994.
(48) Kunkel, G. T.; Maceyka, M.; Milstien, S.; Spiegel, S. Targeting the sphingosine-1-phosphate axis in cancer, inflammation and beyond. *Nat. Rev. Drug Discovery* **2013**, *12*, 688−702.
(49) Al-Abdullah, E. S.; Al-Tuwaijri, H. M.; Hassan, H. M.; Al-Alshaikh, M. A.; Habib, E. E.; El-Emam, A. A. Synthesis, antimicrobial and hypoglycemic activities of novel *N*-(1-adamantyl)carbothioamide derivatives. *Molecules* **2015**, *20*, 8125−8143.
(50) Ju, T.; Gao, D.; Fang, Z. Y. Targeting colorectal cancer cells by a novel sphingosine kinase 1 inhibitor PF-543. *Biochem. Biophys. Res. Commun.* **2016**, *470*, 728−734.
(51) Clark, R. C.; Reid, J. S. The analytical calculation of absorption in multifaceted crystals. *Acta Crystallogr., Sect. A* **1995**, *51*, 887−897.
(52) Dolomanov, O. V.; Bourhis, L. J.; Gildea, R. J.; Howard, J. A. K.; Puschmann, H. OLEX2: A complete structure solution, refinement and analysis program. *J. Appl. Crystallogr.* **2009**, *42*, 339−341.
(53) Sheldrick, G. SHELXT - Integrated space-group and crystal-structure determination. *Acta Crystallogr., Sect. A* **2015**, *71*, 3−8.
(54) Sheldrick, G. Crystal structure refinement with SHELXL. *Acta Crystallogr., Sect. C* **2015**, *71*, 3−8.
(55) Spek, A. Structure validation in chemical crystallography. *Acta Crystallogr., Sect. D* **2009**, *65*, 148−155.
(56) Macrae, C. F.; Sovago, I.; Cottrell, S. J.; Galek, P. T. A.; McCabe, P.; Pidcock, E.; Platings, M.; Shields, G. P.; Stevens, J. S.; Towler, M.; Wood, P. A. Mercury 4.0: From visualization to analysis, design and prediction. *J. Appl. Crystallogr.* **2020**, *53*, 226−235.
(57) Turner, M. J.; Thomas, S. P.; Shi, M. W.; Jayatilaka, D.; Spackman, M. A. Energy frameworks: Insights into interaction anisotropy and the mechanical properties of molecular crystals. *Chem. Commun.* **2015**, *51*, 3735−3738.
(58) Mackenzie, C. F.; Spackman, P. R.; Jayatilaka, D.; Spackman, M. A. CrystalExplorer model energies and energy frameworks: Extension to metal coordination compounds, organic salts, solvates and open-shell systems. *IUCrJ* **2017**, *4*, 575−587.

https://doi.org/10.1021/acsomega.1c03559
ACS Omega 2021, 6, 27026−27037

(59) Turner, M. J.; McKinnon, J. J.; Wolff, S. K.; Grimwood, D. J.; Spackman, P. R.; Jayatilaka, D.; Spackman, M. A. *CrystalExplorer17*; The University of Western Australia Australia, 2017.
(60) Gavezzotti, A. Calculation of lattice energies of organic crystals: The PIXEL integration method in comparison with more traditional methods. *Z. Kristallogr.* **2005**, *220*, 499−510.
(61) Frisch, M. J.; Trucks, G. W.; Schlegel, H. B.; Scuseria, G. E.; Robb, M. A.; Cheeseman, J. R.; Scalmani, G.; Barone, V.; Mennucci, B.; Petersson, G. A.; Nakatsuji, H.; Caricato, M.; Li, X.; Hratchian, H. P.; Izmaylov, A. F.; Bloino, J.; Zheng, G.; Sonnenberg, J. L.; Hada, M.; Ehara, M.; Toyota, K.; Fukuda, R.; Hasegawa, J.; Ishida, M.; Nakajima, T.; Honda, Y.; Kitao, O.; Nakai, H.; Vreven, T.; Montgomery, J. A., Jr.; Peralta, J. E.; Ogliaro, F.; Bearpark, M. J.; Heyd, J.; Brothers, E. N.; Kudin, K. N.; Staroverov, V. N.; Kobayashi, R.; Normand, J.; Raghavachari, K.; Rendell, A. P.; Burant, J. C.; Iyengar, S. S.; Tomasi, J.; Cossi, M.; Rega, N.; Millam, N. J.; Klene, M.; Knox, J. E.; Cross, J. B.; Bakken, V.; Adamo, C.; Jaramillo, J.; Gomperts, R.; Stratmann, R. E.; Yazyev, O.; Austin, A. J.; Cammi, R.; Pomelli, C.; Ochterski, J. W.; Martin, R. L.; Morokuma, K.; Zakrzewski, V. G.; Voth, G. A.; Salvador, P.; Dannenberg, J. J.; Dapprich, S.; Daniels, A. D.; Farkas, Ö.; Foresman, J. B.; Ortiz, J. V.; Cioslowski, J.; Fox, D. J. *Gaussian 09, revision D.01;* Gaussian, Inc.: Wallingford, CT, 2013.
(62) Boys, S. F.; Bernardi, F. The calculation of small molecular interactions by the differences of separate total energies. Some procedures with reduced errors. *Mol. Phys.* **1970**, *19*, 553−566.
(63) Keith, T. A. *AIMAll*, Ver. 19.02.13; TK Gristmill Software: Overland Park, KS, 2019.

https://doi.org/10.1021/acsomega.1c03559
ACS Omega 2021, 6, 27026−27037